Supplemental Material: Nonadiabatic Born effective charges in metals

Cyrus E. Dreyer,[1, 2] Sinisa Coh,[3] and Massimiliano Stengel[4, 5]

[1]*Department of Physics and Astronomy, Stony Brook University, Stony Brook, New York, 11794-3800, USA*
[2]*Center for Computational Quantum Physics, Flatiron Institute,*
162 5th Avenue, New York, New York 10010, USA
[3]*Materials Science and Mechanical Engineering, University of California Riverside, CA 92521, USA*
[4]*Institut de Ciència de Materials de Barcelona (ICMAB-CSIC), Campus UAB, 08193 Bellaterra, Spain*
[5]*ICREA-Institució Catalana de Recerca i Estudis Avançats, 08010 Barcelona, Spain*
(Dated: January 26, 2022)

S1. DETAILS OF DFPT FORMALISM

We will perform our derivation and ultimately our calculations in the framework of planewave/pseudopotential Kohn-Sham[S1] DFT. Thus $\psi_{n\mathbf{k}}(\mathbf{r}) = u_{n\mathbf{k}}(\mathbf{r})e^{i\mathbf{k}\cdot\mathbf{r}}$ corresponds to the single-particle wavefunction of band n and wavevector $\mathbf{k}$ in the first Brillouin zone that is the solution of the Kohn-Sham equation with the single particle Hamiltonian

$$\hat{\mathcal{H}} = \hat{T} + \hat{V}_{\text{Hxc}}[\rho] + \hat{V}_{\text{ext}}, \tag{S1}$$

where $\hat{T}$ is the single-particle kinetic energy, $\hat{V}_{\text{Hxc}}[\rho]$ denotes the Hartree and exchange-correlation (Hxc) potential, which is a functional of the density ρ, and $\hat{V}_{\text{ext}}$ is the external potential that includes the pseudopotential operators (local and nonlocal). We will often use the "cell-periodic" version of operators: $\hat{\mathcal{O}}_{\mathbf{k}} = e^{-i\mathbf{k}\cdot\mathbf{r}}\hat{\mathcal{O}}e^{i\mathbf{k}\cdot\mathbf{r}}$ which operate on the cell-periodic functions $u_{n\mathbf{k}}(\mathbf{r})$.

A. Generalized susceptibility

We begin with the generalized susceptibility introduced in the main text, and partition it in the following way

$$\chi^{\text{na}}_{\lambda_1\lambda_2}(\omega, \mathbf{q}) = \chi^{\text{geom}}_{\lambda_1\lambda_2}(\mathbf{q}) + \chi^{\text{Kubo}}_{\lambda_1\lambda_2}(\omega, \mathbf{q}). \tag{S2}$$

The "geometric" contribution only depends on the unperturbed density operator, $\hat{\rho}$, and is independent of ω. Taking immediately the limit of $\mathbf{q} \to 0$,

$$\chi^{\text{geom}}_{\lambda_1\lambda_2} = \text{Tr}\left(\hat{H}^{\lambda_1\lambda_2}_{\mathbf{k}}\hat{\rho}\right), \quad \hat{\rho}_{\mathbf{k}} = \sum_n |u_{n\mathbf{k}}\rangle f_{n\mathbf{k}}\langle u_{n\mathbf{k}}|, \tag{S3}$$

where $\hat{H}^{\lambda_1\lambda_2}_{\mathbf{k}} = \partial^2 \hat{H}_{\mathbf{k}}/\partial\lambda_1\partial\lambda_2$ is the second derivative of the external potential (i.e., not containing the SCF part), and $f_{n\mathbf{k}}$ is the occupation of band n at k-point $\mathbf{k}$. Note that the trace implicitly consists of a sum over bands and Brillouin-zone average,

$$\text{Tr}\left(\hat{A}\hat{B}\right) = \int [d^3k] \sum_{mn} \langle u_{m\mathbf{k}}|\hat{A}_{\mathbf{k}}|u_{n\mathbf{k}}\rangle\langle u_{n\mathbf{k}}|\hat{B}_{\mathbf{k}}|u_{m\mathbf{k}}\rangle. \tag{S4}$$

The second term in Eq. (S2) can be written as

$$\chi^{\text{Kubo}}_{\lambda_1\lambda_2}(\omega, \mathbf{q}) = \text{Tr}\left[\hat{H}^{\lambda_1\dagger}_{\mathbf{k},\mathbf{q}}\hat{\rho}^{\lambda_2}(\omega, \mathbf{q})\right], \tag{S5}$$

where the first-order density matrix is written as a double sum over states

$$\hat{\rho}^{\lambda}_{\mathbf{k}}(\omega, \mathbf{q}) = \lim_{\eta\to 0} \sum_{nm} \bar{f}_{nm\mathbf{k}}(\omega + i\eta, \mathbf{q})|u_{m\mathbf{k}+\mathbf{q}}\rangle\langle u_{m\mathbf{k}+\mathbf{q}}|\hat{\mathcal{H}}^{\lambda}_{\mathbf{k},\mathbf{q}}(\omega)|u_{n\mathbf{k}}\rangle\langle u_{n\mathbf{k}}|, \tag{S6}$$

with

$$\bar{f}_{nm\mathbf{k}}(z, \mathbf{q}) = \frac{f_{n\mathbf{k}} - f_{m\mathbf{k}+\mathbf{q}}}{\epsilon_{n\mathbf{k}} - \epsilon_{m\mathbf{k}+\mathbf{q}} + z}. \tag{S7}$$

Note that the first-order Hamiltonian becomes ω-dependent via the charge self-consistency once the local fields are incorporated,

$$\hat{\mathcal{H}}^\lambda(\omega) = \hat{H}^\lambda + \hat{V}^\lambda_{\text{Hxc}}(\omega) \tag{S8}$$

where $\hat{H}^\lambda$ is the kinetic energy and external potential perturbation, and $\hat{V}^\lambda_{\text{Hxc}}$ is the potential response containing self-consistent fields (SCF) that depends on the first-order density, $\rho^\lambda_{\mathbf{q}}(\mathbf{r}, \omega) = \langle \mathbf{r} | \hat{\rho}^{\lambda_2}(\omega, \mathbf{q}) | \mathbf{r} \rangle$ as

$$\hat{V}^\lambda_{\text{Hxc}}(\mathbf{r}, \omega) = \int d^3 r' K_{\text{Hxc}}(\mathbf{r}, \mathbf{r}') \rho^{\lambda, \omega}(\mathbf{r}, \omega), \tag{S9}$$

where K_{Hxc} is the Hxc kernel, defined as the variation of the SCF potential with respect to a charge-density perturbation.

B. Adiabatic regime

If we take $\omega \to 0$, the intraband contribution in Eq. (S5) remains finite, and

$$\overline{f}_{nn\mathbf{k}} \to \left. \frac{df(\epsilon)}{d\epsilon} \right|_{\epsilon = \epsilon_{n\mathbf{k}}}. \tag{S10}$$

Then, for a $\mathbf{q} = 0$ perturbation, we obtain the *adiabatic* response,

$$\chi^{\text{ad}}_{\lambda_1 \lambda_2} = \text{Tr}\left[\frac{\partial}{\partial \lambda_2}\left(\hat{\rho} \hat{H}^{\lambda_1} \right) \right]. \tag{S11}$$

Note that $\chi^{\text{ad}}_{\lambda_1 \lambda_2}$ is written as a total derivative with respect to one of the perturbations. This means that, if either the λ_1 or λ_2 is a vector potential field, the corresponding perturbation reduces to a partial derivative with respect to k_α, and its BZ average vanishes. Physically, the fact that $\chi^{\text{ad}}_{A_\alpha A_\beta}$ vanishes is a direct consequence of the f-sum rule; the result $\chi^{\text{ad}}_{A_\alpha \tau_{\kappa\beta}} = 0$, on the other hand, tells us that a static atomic displacement cannot produce a steady current. $\chi^{\text{ad}}_{\tau_{\kappa\alpha} \tau_{\kappa'\beta}}$ does not vanish: it is the electronic contribution to the adiabatic force-constant matrix, as it is calculated in most linear-response DFT packages.[S2–S4]

C. Nonadiabatic response

When considering, e.g., optical phonons in polar crystal lattices, or the response to electromagnetic radiation, it is appropriate to reverse the order of the $\mathbf{q} \to 0$ and $\omega \to 0$ limits. The intraband contributions to Eq. (S5) is suppressed in the $\mathbf{q} \to 0$ limit, thus, we obtain a *nonadiabatic* response function as the *interband* part of the adiabatic one, i.e., by replacing $\hat{\rho}^{\lambda_2}$ in Eq. (S5) with

$$\hat{\rho}^{\lambda_2, \text{inter}}_{\mathbf{k}} = \sum_{n \neq m} \overline{f}^{\mathbf{k}}_{nm} |u_{m\mathbf{k}}\rangle \langle u_{m\mathbf{k}} | \hat{\mathcal{H}}^{\lambda_2}_{\mathbf{k}} | u_{n\mathbf{k}}\rangle \langle u_{n\mathbf{k}}|. \tag{S12}$$

Note that, in principle, the intraband contribution to the first-order charge density should be removed as well, i.e., the adiabatic scattering potential $\hat{\mathcal{H}}^{\lambda_2}$ should be replaced with $\hat{\mathcal{H}}^{\lambda_2, \text{inter}} = \hat{H}^{\lambda_2} + \hat{V}^{\lambda_2, \text{inter}}_{\text{Hxc}}$, and $\hat{V}^{\lambda_2, \text{inter}}_{\text{Hxc}}$ is defined from $\rho^{\lambda_2, \text{inter}}(\mathbf{r})$ via Eq. (S9). While taking this extra step would be desirable, as it would lead to a fully self-consistent computational setup, it would also substantially complicate the implementation; therefore, in our calculations we have retained the adiabatic phonon perturbation, $\hat{\mathcal{H}}^{\lambda_2}$, for simplicity. We believe, in fact, that our calculations are unaffected by such a simplifying assumption, as we shall clarify in the following.

At small (but finite) $\mathbf{q}$, correctly treating the intraband contribution to the density in the SCF cycles may be important. Whether free carriers participate (full adiabatic density) or do not participate (nonadiabatic interband-only density) to screening a phonon perturbation has obviously a crucial impact on the macroscopic electric fields that are produced, e.g., by a long-wavelength LO mode. Right at the zone center, however, and under the assumption of short-circuit electrical boundary conditions (as required by the definition of the Born dynamical charge tensor), neglecting the nonadiabatic correction to the SCF potential is much safer, since it may only lead to a small discrepancy

in the first-order potential that averages to zero over the cell. Furthermore, in presence of space-inversion symmetry, infrared-active modes (i.e., the only ones carrying a nonzero dynamical charge) do not couple with Fermi-level shifts, and hence their intraband contribution to the density response should vanish. This indicates that our calculations (all performed on centrosymmetric crystals) should not be affected by this issue.

1. Drude weight

Consider the case where both λ_1 and λ_2 are components of the vector potential. The total density response to a translation in $\mathbf{k}$-space vanishes, so the interband contribution to the density response is minus the intraband one. Also, the density response, and thus the SCF contributions vanish if TRS is present (since $\overline{f}_{nn\mathbf{k}}$ and $|u_{n\mathbf{k}}(\mathbf{r})|^2$ are even under $\mathbf{k} \to -\mathbf{k}$, while $\langle u_{n\mathbf{k}}|\hat{H}_{\mathbf{k}}^{A_\alpha}|u_{n\mathbf{k}}\rangle$ is odd). Thus, the response reduces to the familiar Drude expression (e.g, see Ref. S5),

$$
\begin{aligned}
\chi_{A_\alpha A_\beta}^{\mathrm{na}} &= -\int [d^3k]\overline{f}_{nn\mathbf{k}}\langle u_{n\mathbf{k}}|\hat{H}_{\mathbf{k}}^{A_\alpha}|u_{n\mathbf{k}}\rangle\langle u_{n\mathbf{k}}|\hat{H}_{\mathbf{k}}^{A_\beta}|u_{n\mathbf{k}}\rangle \\
&= -\int [d^3k]\overline{f}_{nn\mathbf{k}}\frac{\partial \epsilon_{n\mathbf{k}}}{\partial k_\alpha}\frac{\partial \epsilon_{n\mathbf{k}}}{\partial k_\beta} = \frac{\Omega}{\pi}D_{\alpha\beta},
\end{aligned}
\tag{S13}
$$

where Ω is the cell volume. $D_{\alpha\beta}$ is the "Drude weight." This corresponds to the optical conductivity multiplied by $i\omega$. The Drude weight is nonzero in all metals, regardless of crystal symmetry, which is seen by realizing that the square of the Fermi velocities in Eq. (S13) is even under $\mathbf{k} \to -\mathbf{k}$ even if the crystal has TR and inversion symmetry.

As discussed in the main text, we will also consider a "modified" version of the Drude weight, given by

$$
\frac{\Omega}{\pi}\widetilde{D}_{\alpha\beta} = -\int [d^3k]\overline{f}_{nn\mathbf{k}}\langle u_{n\mathbf{k}}|\hat{H}_{\mathbf{k}}^{A_\alpha}|u_{n\mathbf{k}}\rangle\langle u_{n\mathbf{k}}|\hat{p}_{\beta\mathbf{k}}|u_{n\mathbf{k}}\rangle
\tag{S14}
$$

where $\hat{p}_{\beta,\mathbf{k}} = -i\nabla_\beta + \hat{k}_\beta$ is the canonical momentum operator.

2. Born effective charges

We will now derive the nonadiabatic response at first order in the velocity, valid for the optical conductivity and the Born effective charges. The derivation rests on the following identity

$$
\frac{\Delta f}{\Delta \epsilon + z} = \frac{\Delta f}{\Delta \epsilon}\left(1 - \frac{z}{\Delta \epsilon + z}\right).
\tag{S15}
$$

The first term in the round brackets does not depend on frequency; summed with the geometric term it yields the adiabatic response, which vanishes both for the current–current and the current–force response functions. From the second term in the round brackets we readily obtain, via Eq. (1) of the main text, the established formula for the optical conductivity (i.e., Eq. (25) of Ref. S6). Similarly, Eq. (2) of the main text yields the electronic contribution to the Born charges as[S7,S8]

$$
Z_{\kappa\beta}^{(\alpha)}(\omega + i\eta), = -\frac{1}{i}\int [d^3k]\sum_{nm}\frac{\overline{f}_{nm\mathbf{k}}}{\epsilon_{n\mathbf{k}} - \epsilon_{m\mathbf{k}} + z}\langle u_{n\mathbf{k}}\hat{H}_{\mathbf{k}}^{k_\alpha\dagger}|u_{m\mathbf{k}}\rangle\langle u_{m\mathbf{k}}|\hat{\mathcal{H}}_{\mathbf{k}}^{\tau_\beta}(z)|u_{n\mathbf{k}}\rangle,
\tag{S16}
$$

where $\hat{H}_{\mathbf{k}}^{k_\alpha}$ is the velocity operator and $\tau_{\kappa\beta}$ indicates the displacement of the sublattice κ along the Cartesian direction β. After taking the $\omega \to 0$ limit, we readily obtain the expression for the naBEC given by Eq. (7) of the main text. In an insulator, Eq. (7) reduces to the usual expressions for the adiabatic BEC.

D. Sums over empty states

If we were to calculate the naBEC using Eq. (7), then we would have to perform a convergence over empty states. In order to avoid this, we will use the same approach as is common in DFPT, casting the problem in terms of obtaining first-order wavefunctions via solving a Sternheimer equation. To this end, we shall assume that the active subspace of states that are treated explicitly in the calculation spans the lowest M orbitals with occupation numbers different

from zero. Then, we can decompose Eq. (7) into a double sum over the first M states plus two sums over $1, \ldots, M$ and $M + 1, \ldots,$

$$
\begin{aligned}
&\lim_{\eta \to 0^+} \int [d^3k] \sum_{n \leq M, m \leq M} \frac{\overline{f}_{nm\mathbf{k}}}{\epsilon_{n\mathbf{k}} - \epsilon_{m\mathbf{k}} + i\eta} \langle u_{n\mathbf{k}}|\hat{H}_{\mathbf{k}}^{k_\alpha}|u_{m\mathbf{k}}\rangle \langle u_{m\mathbf{k}}|\hat{\mathcal{H}}_{\mathbf{k}}^{\tau_{\kappa\beta},\text{inter}}|u_{n\mathbf{k}}\rangle \\
&+ \int [d^3k] \sum_{n \leq M, m \geq M+1} \frac{f_{n\mathbf{k}}}{(\epsilon_{n\mathbf{k}} - \epsilon_{m\mathbf{k}})^2} \langle u_{n\mathbf{k}}|\hat{H}_{\mathbf{k}}^{k_\alpha}|u_{m\mathbf{k}}\rangle \langle u_{m\mathbf{k}}|\hat{\mathcal{H}}_{\mathbf{k}}^{\tau_{\kappa\beta},\text{inter}}|u_{n\mathbf{k}}\rangle \\
&- \int [d^3k] \sum_{m \leq M, n \geq M+1} \frac{f_{m\mathbf{k}}}{(\epsilon_{n\mathbf{k}} - \epsilon_{m\mathbf{k}})^2} \langle u_{n\mathbf{k}}|\hat{H}_{\mathbf{k}}^{k_\alpha}|u_{m\mathbf{k}}\rangle \langle u_{m\mathbf{k}}|\hat{\mathcal{H}}_{\mathbf{k}}^{\tau_{\kappa\beta},\text{inter}}|u_{n\mathbf{k}}\rangle
\end{aligned}
\tag{S17}
$$

The second and third terms can be conveniently rewritten as a Berry curvature in parameter space, so the naBEC can be written as

$$
\begin{aligned}
Z^*_{\alpha,\kappa\beta} = Z^{\text{ion}}_\kappa \delta_{\alpha\beta} - \text{Im} &\Bigg[\int [d^3k] \sum_{n \leq M} f_{n\mathbf{k}} \left(\langle u_{n\mathbf{k}}^{k_\alpha}|u_{n\mathbf{k}}^{\tau_{\kappa\beta},\text{inter}}\rangle - \langle u_{n\mathbf{k}}^{\tau_{\kappa\beta},\text{inter}}|u_{n\mathbf{k}}^{k_\alpha}\rangle \right) \\
&+ \lim_{\eta \to 0^+} \int [d^3k] \sum_{n \leq M, m \leq M} \frac{\overline{f}_{nm\mathbf{k}}}{\epsilon_{n\mathbf{k}} - \epsilon_{m\mathbf{k}} + i\eta} \langle u_{n\mathbf{k}}|\hat{H}_{\mathbf{k}}^{k_\alpha}|u_{m\mathbf{k}}\rangle \langle u_{m\mathbf{k}}|\hat{\mathcal{H}}_{\mathbf{k}}^{\tau_{\kappa\beta},\text{inter}}|u_{n\mathbf{k}}\rangle \Bigg]
\end{aligned}
\tag{S18}
$$

where the first-order wavefunctions are defined via

$$
(\hat{\mathcal{H}}_{\mathbf{k}} + a\hat{P}_{\mathbf{k}}^M - \epsilon_{n\mathbf{k}})|u_{n\mathbf{k}}^\lambda\rangle = -\hat{Q}_{\mathbf{k}}^M \hat{\mathcal{H}}_{\mathbf{k}}^\lambda |u_{n\mathbf{k}}\rangle,
\tag{S19}
$$

where $\hat{P}_{\mathbf{k}}^M - \sum_n^M |u_{n\mathbf{k}}\rangle\langle u_{m\mathbf{k}}|$ and $\hat{Q}_{\mathbf{k}}^M = 1 - \hat{P}_{\mathbf{k}}$ are projectors inside and outside the active space, and a is a constant that needs to be larger than the total bandwidth of the active space. Eq. (S19) has the same form as the Sternheimer equation solved presently in DFPT implementations,[S2–S4] except that $\hat{P}_{\mathbf{k}}^M$ does not correspond to the ground-state density operator, but instead the projector over an "active space" M, which is chosen to be large enough to encompass all states such that the occupation of the Mth band vanishes. We will show in Sec. S1 D that the choice of M does not influence the final result.

S2. COMPUTATIONAL APPROACH AND CONVERGENCE

A. Computational parameters

We implemented the methodology for calculating the naBEC and DW in the ABINIT package,[S9] taking advantage of the DFPT implementation for calculating the (static) response to atomic displacements and infinitesimal electric fields.[S3,S4] In all cases, η is fixed to be 10^{-5} Ha. Optimized Vanderbilt norm-conserving pseudopotentials[S10] taken from PSEUDO-DOJO are used for all calculations.

For Al, we use the PBE[S11] generalized-gradient approximation exchange-correlation functional, as it provides better structural properties compared to LDA (cubic lattice parameter of 7.63 Bohr). We use Fermi-Dirac smearing with a "temperature" of 0.005 Ha. As mentioned in the main text, k-meshes up to $28 \times 28 \times 28$ were used. For the calculation of the naBEC, we used an active space of $M = 40$ bands; we show in Fig. S1 that the total naBEC does not depend on such choice, as long as enough bands are included such that the occupation of the highest band is negligible ($M \geq 20$ for the conventional cubic cell).

For cubic ($Pm\overline{3}m$) SrTiO$_3$ (STO) and SnS$_2$, the local density approximation (LDA) functional parametrized in Ref. S12 was used (as they provide better structural properties than GGA for these materials). The relaxed lattice parameter(s) for STO was 7.29 Bohr and for SnS$_2$ were $a = 6.87$ and $c = 10.78$ Bohr. Gaussian smearing was used with a width of 0.005 Ha, and a "coarse" k-mesh of $8 \times 8 \times 8$ was used for the undoped calculations for STO and 0.001 Ha and $12 \times 12 \times 6$ for SnS$_2$. (The slightly larger smearing for STO was in order to smooth fluctuations due to the sharp features in the Fermi surface, see Sec. S2 D) The linear response quantities necessary for the calculation of the naBEC and DW with electron doping were Wannier interpolated onto a "fine" mesh in k space as discussed in Sec. S2 B.
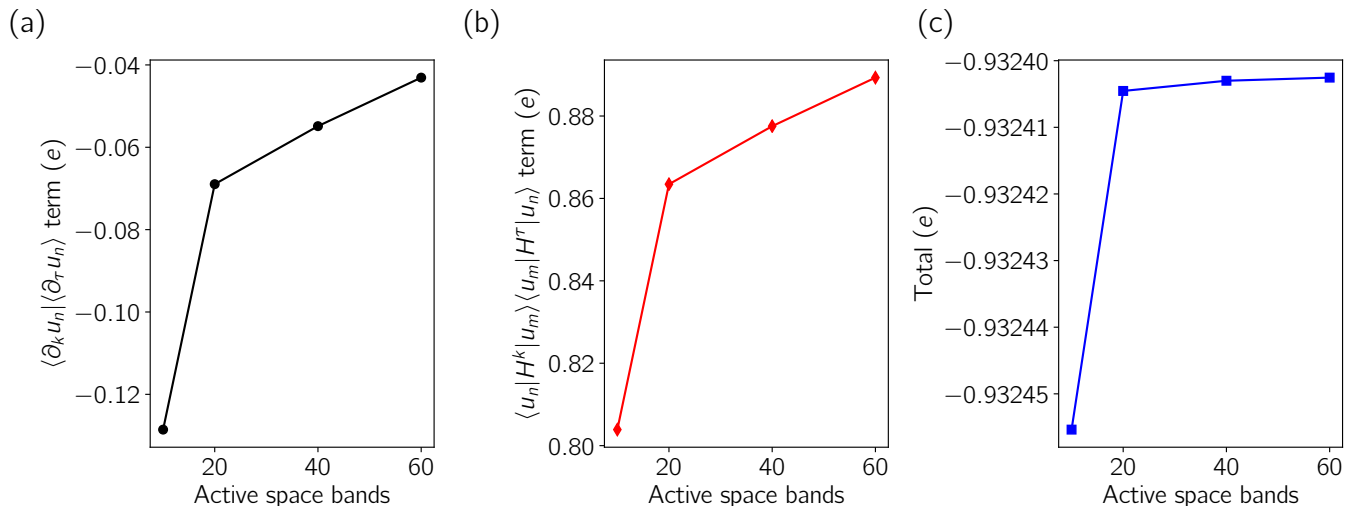
FIG. S1: For cubic cell of FCC Al, the dependence on choice of number of bands in the "active space" M of (a) the second term in Eq. (S18), (b) the third term in Eq. (S18), (c) the total electronic contribution to the nonadiabatic Born effective charge.
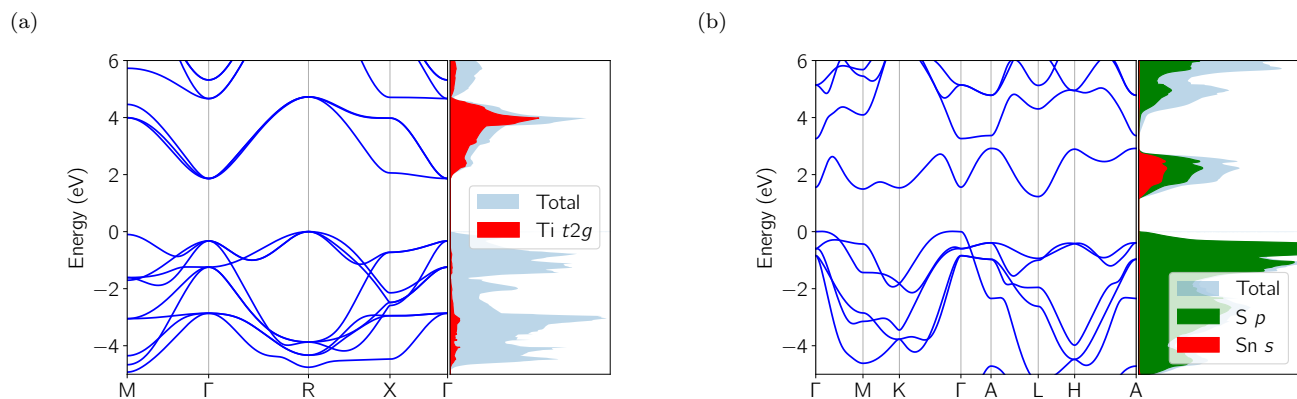

FIG. S2: Bandstructure and projected density of states (DOS) for (a) $Pm\overline{3}m$ SrTiO$_3$ and (b) SnS$_2$. Zero energy for each is set to the top of the valence band.

B. First-order Wannier functions for interpolation

In order to achieve the meshes in k space necessary to converge the naBEC and DW for the doped semiconductors STO and SnS$_2$ (see the next section for discussion of the doping), we performed a Wannier interpolation of the quantities in Eqs. (S18), and (S13). Maximally-localized Wannier functions are generated using the WANNIER90[S13] interface with ABINIT for the valence bands as well as the three lowest-lying conduction bands for STO [Fig. S2(a)], and single lowest-lying conduction band for SnS$_2$ [Fig. S2(b)]. In order to ensure that the a consistent gauge is used, DFPT calculations are initiated from the same ground-state wavefunctions as used for the Wannierization. The unitary transformations that produced the Wannier functions of the ground-state Hamiltonian are used to interpolate the first-order Hamiltonian and wavefunction derivatives (a similar strategy as employed in Refs. S14 and S15) onto a fine k-mesh. In order to confirm that this procedure is providing a valid localized basis for interpolation, we plot the decay of the ground state and first-order Hamiltonian matrix elements for STO in real space in Fig. S3 (a similar behavior is observed for SnS$_2$). For the results in the main text, we use a fine mesh of $100 \times 100 \times 100$ for STO, and $128 \times 128 \times 64$ for SnS$_2$.
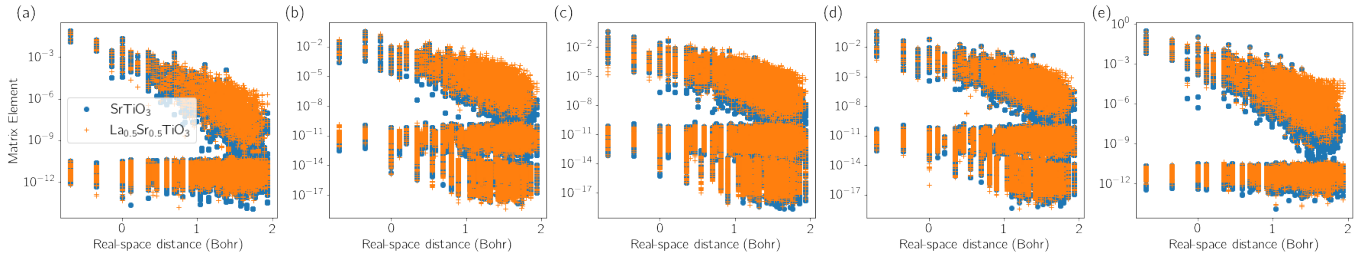
FIG. S3: Decay of the real-space matrix elements of (a) the ground state Hamiltonian, (b) atomic displacement perturbations, (c) velocity operator, (d) momentum operator, and (e), the matrix elements involved in the second term in Eq. (S18). Blue circles are for undoped STO, orange crosses are doped with La ($0.5e$ per cell) via the virtual crystal approximation.
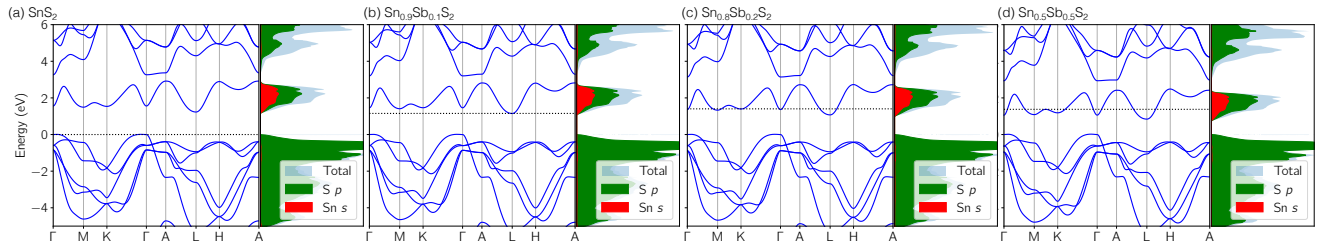

FIG. S4: Band structure using the virtual crystal approximation for $Sb_xSn_{1-x}S_2$ with various Sb concentrations. Dotted line is the Fermi level, and energy zero is set to the top of the valence band in all cases.

C. Electron doping

For Figs. 2 and 3 in the main text, SnS_2 and STO were doped via the rigid-band approximation, i.e., only the occupation factors were changed with Fermi level. For STO, doping was performed across the entire Ti $3d$ t_{2g} conduction band manifold [see Fig. S2(a)], while for SnS_2, the doping was performed across the single conduction band [see Fig. S2(b)], which has S $3p$ and Sn $5s$ character.

We can explore the accuracy of this approximation by comparing with explicit doping via the virtual-crystal approximation (VCA). To do this, the Sn (Sr) pseudopotential was alchemically mixed with a Sb (La) pseudopotential, with all structural properties kept fixed. The same Wannier interpolation procedure (Sec. S2 B) was used in these cases
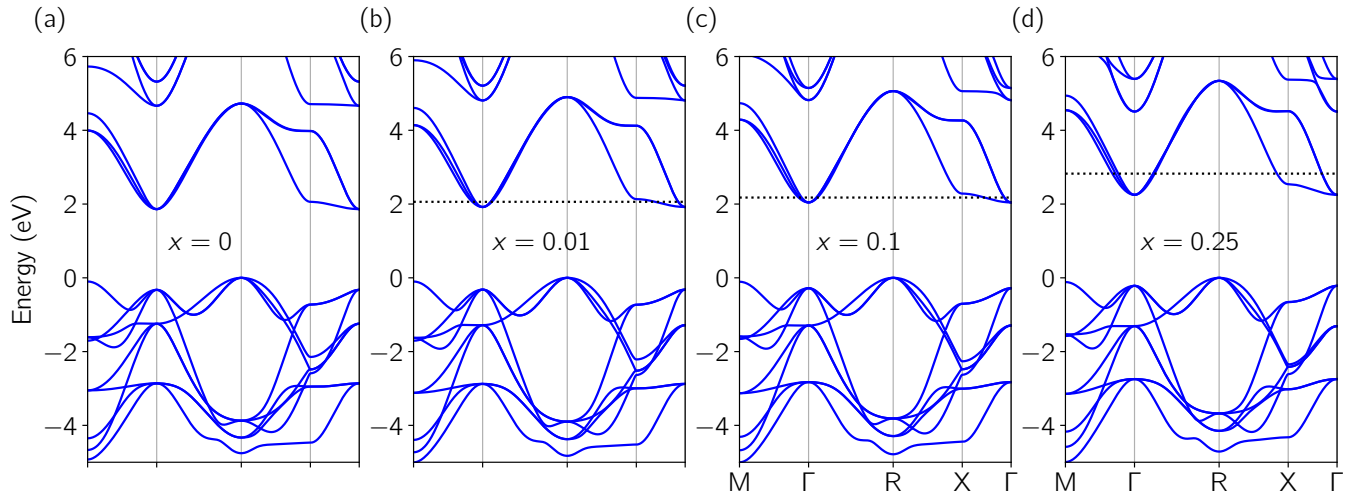

FIG. S5: Band structure using the virtual crystal approximation for $La_xSr_{1-x}TiO_3$ with various La concentrations. Dotted line is the Fermi level, and energy zero is set to the top of the valence band in all cases.
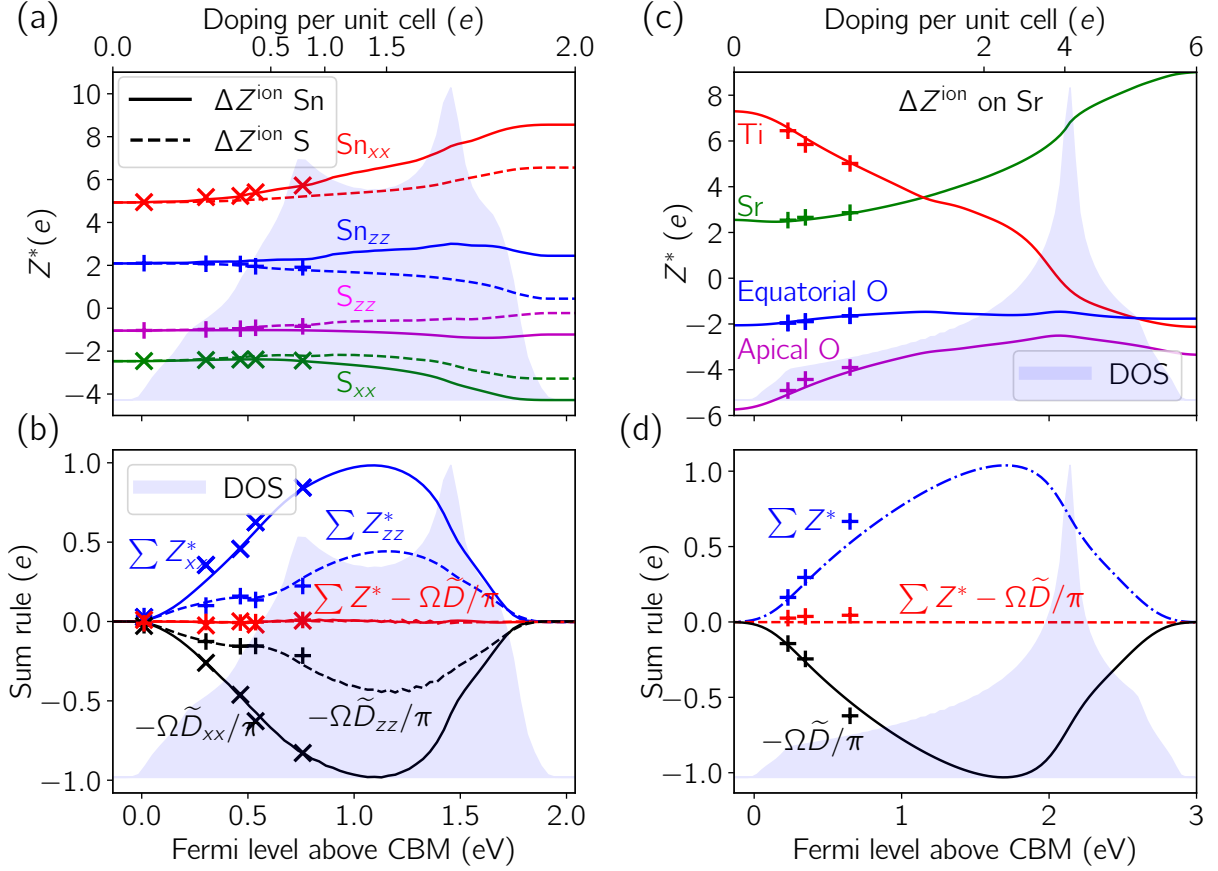
FIG. S6: Comparison of explicit doping via the virtual-crystal approximation (+'s and x's) and the rigid-band approximation (curves, same as Figs. 2 and 3 in the main text). Points in (a) and (b) are obtained by alchemically mixing the Sn pseudopotential with Sb, and in (c) and (d) mixing Sr with La.

as in the rigid-band calculations. In Figs. S4 and S5, we show that the band structures do not change significantly with doping via VCA (as long as the structural parameters are fixed). From, e.g., Fig. S4(d), we do see some subtle changes at large doping for SnS_2, i.e., it can be seen from the DOS that as the S p/Sn s conduction band is filled, the splitting to the S p valence band decreases slightly.

In Fig. S3 we compare the ground state (panel a) and first-order matrix elements that make up the naBEC and Drude weight (panels b-e) calculated for undoped STO (blue circles) and VCA $La_{0.5}Sr_{0.5}Ti_3$ (orange crosses). Overall, there is good agreement between the two cases, even for such a large doping; the spatial decay is somewhat reduced for the VCA doped case, which is likely due to slightly less localized Wannier functions in the metallic case.

In Fig. S6 we compare the naBECs and sum rule for SnS_2 and STO calculated with the VCA (points) and rigid-band approximations (curves, same as Figs. 2 and 3 in the main text). We can see that the agreement is excellent at low doping. At higher doping there are some quantitative differences. In the case of SnS_2, there are some small deviations at 50% Sb doping in the z components of the naBEC; for STO at 50% La doping, the total naBEC and Drude weight are slightly larger than for the rigid-band approximation. However, crucially, the naBEC sum rule is accurately satisfied in both cases, and thus does not depend on how we apply the doping. The increased scatter in the VCA points does indicate more challenging convergence when the dopant electrons are explicitly included.

D. Convergence of nonadiabatic Born effective charges and Drude Weight

In this section we explore the numerical convergence of the naBECs and DW. In Fig. S7 we plot the convergence of the electronic part of the naBECs with interpolated k mesh. We plot separately the second [Fig. S7(a)] and third [Fig. S7(b)] terms in Eq. (S18) (the first ionic term is not included). We can see that the third term, which is nonzero only when empty bands are included in the active space, is the most difficult to converge especially as the van Hove
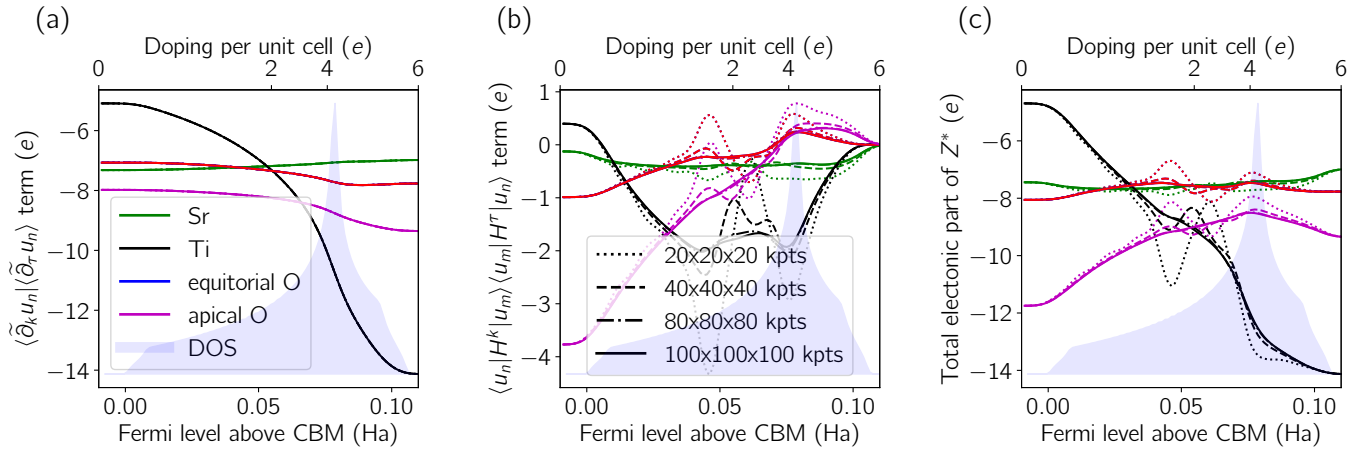
FIG. S7: Convergence of the electronic part of the naBECs of STO with interpolated k mesh. (a) is the second term in Eq. (S18), (b) is the third term in Eq. (S18), and (c) is the total electronic contribution to the nonadiabatic Born effective charge. The density of states of the Ti $t2g$ manifold is superimposed, and the thermal smearing is set to $\sigma = 0.005$ Ha.
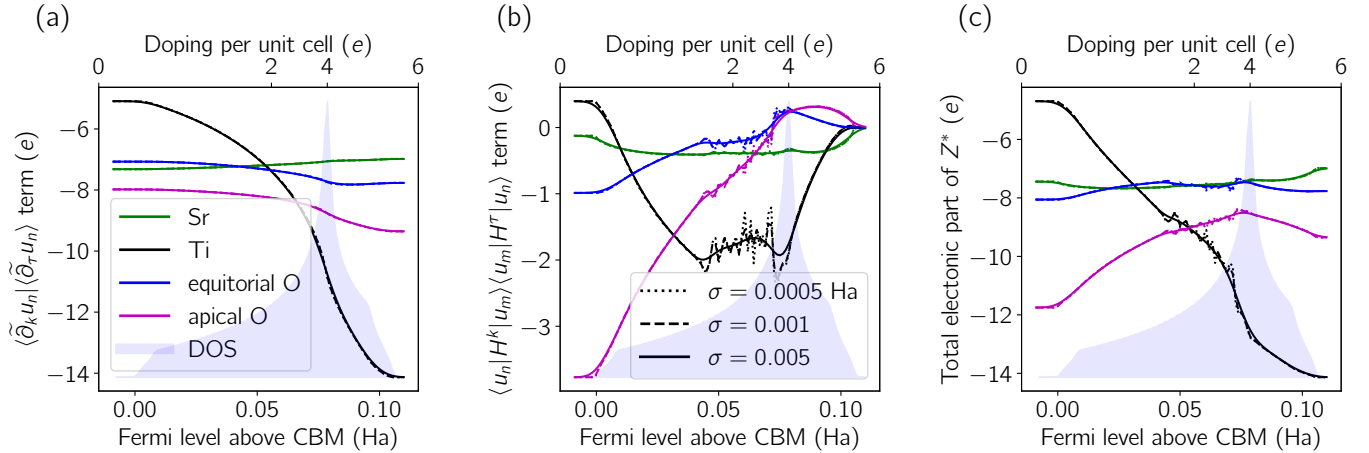

FIG. S8: Same as Fig. S7, demonstrating convergence with respect to thermal spearing, σ (k mesh is fixed to $100 \times 100 \times 100$).

singularity (vHS) is approached. In Fig. S8, we plot the convergence of the naBEC for STO with respect to the width of the Gaussian smearing σ. Similarly to the case with k mesh, the third term in Eq. (S18) shows oscillations for lower meshes as the vHS is approached, that are smoothed with larger smearings. These oscillations could also be removed with larger k meshes.

We turn now to the convergence of Drude weight (DW), and the naBEC sum rule. In the main text, two versions of of the DW are discussed, i.e., whether the perturbation and response are both taken to be the *velocity* operators ("velocity-velocity", which we will denote here as D), or the velocity operator and *momentum* operator ("velocity-momentum", which we will denote here as $\widetilde{D}$). The velocity and momentum operators differ in our density-functional theory calculations since the pseudopotentials contain nonlocal potentials.[S16–S19]

In Fig. S9(a) we plot the sublattice sum of the naBEC (including the ionic contribution) for different interpolated k meshes; we see that this sum converges quite rapidly. In Fig. S9(b) and (c) we demonstrate the naBEC sum rule. This also converges quickly with k-mesh. Also, we clearly see that the standard DW violates the naBEC sum rule, which is accurately satisfied by the $\widetilde{D}$ version. In Fig. S10, we plot the convergence of the same quantities with the smearing. As with the naBECs, we see that a σ of 0.005 Ha is required to smooth the oscillations in the sum rule for a k mesh of $100 \times 100 \times 100$. A larger mesh would allow us to use a smaller smearing.

The convergence behavior is overall quite similar for SnS$_2$. For example, in Fig. S11 we show the convergence of the naBEC sum rule with interpolated k mesh for both the $\alpha = \beta = \hat{x}$ [Fig. S11(a)-(c)] and $\alpha = \beta = \hat{z}$ [Fig. S11(d)-(f)]
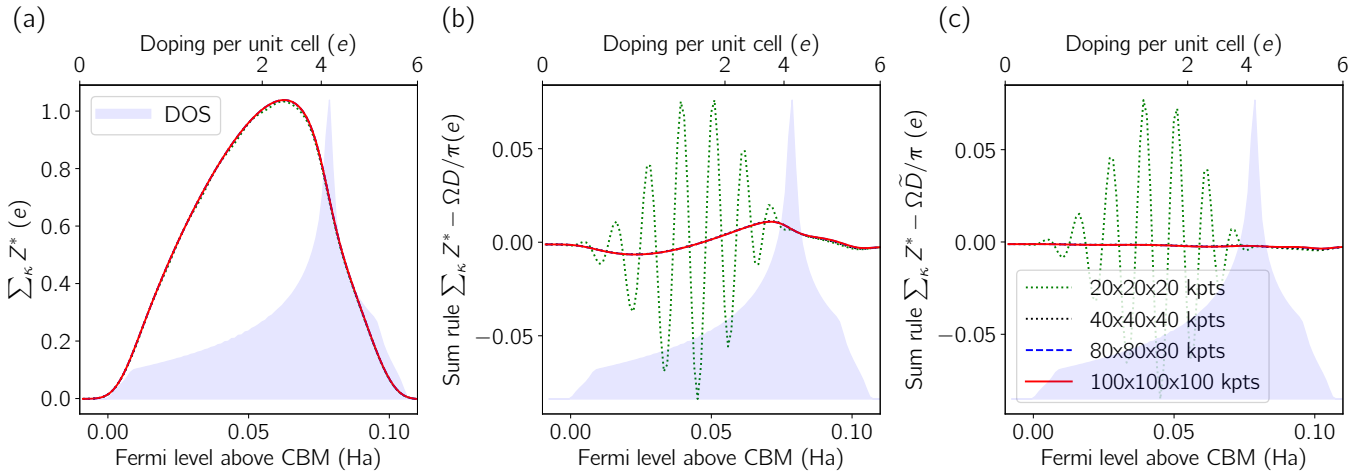
FIG. S9: (a) Sum of nonadiabatic Born effective charges (naBECs), (b) sum of naBECs and standard velocity-velocity Drude weight (DW), (c) sum of naBECs and modified momentum-velocity version of DW, for different k meshes, with the density of states of the Ti $t2g$ manifold superimposed. We set the thermal smearing to $\sigma = 0.005$ Ha
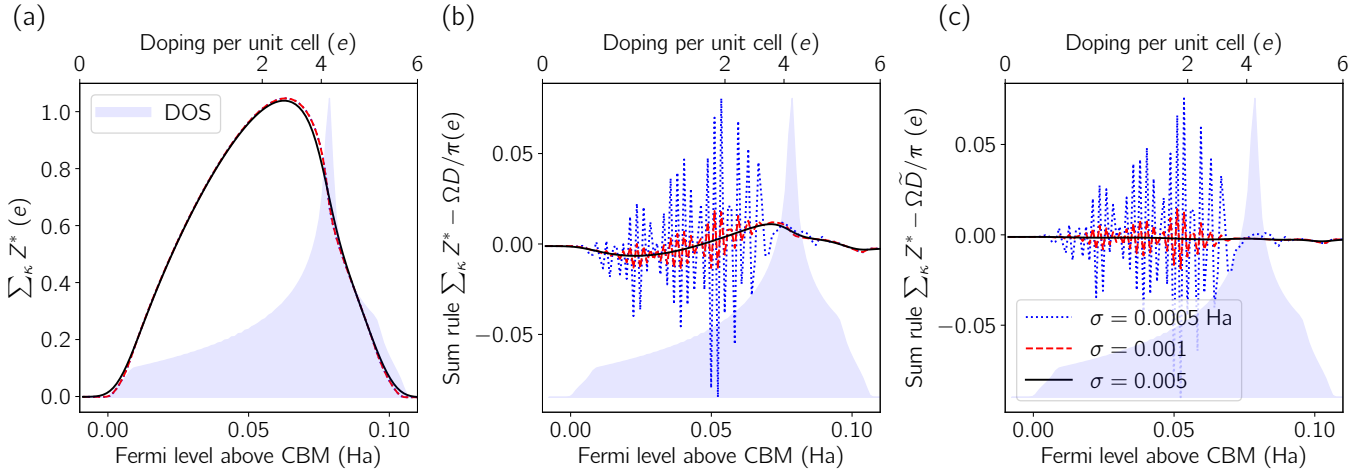

FIG. S10: Same as Fig. S9, but for different values of the thermal smearing σ with the k-mesh set to $100 \times 100 \times 100$.

components. We see the same behavior as for STO, where the naBEC sum rule is most accurately satisfied for the $\widetilde{D}$ version of the DW.

[S1] W. Kohn and L. J. Sham, Phys. Rev. **140**, A1133 (1965).

[S2] S. Baroni, S. de Gironcoli, A. Dal Corso, and P. Giannozzi, Rev. Mod. Phys. **73**, 515 (2001).

[S3] X. Gonze, Phys. Rev. B **55**, 10337 (1997).

[S4] X. Gonze and C. Lee, Phys. Rev. B **55**, 10355 (1997).

[S5] R. Resta, J. Phys. Condens. Mat. **30**, aade19 (2018).

[S6] P. B. Allen, in *Conceptual Foundations of Materials: A Standard Model for Ground- and Excited-State Properties*, edited by S. G. Louie and M. L. Cohen (Elsevier B.V., Amsterdam, The Netherlands, 1993) Chap. 6, pp. 165–218.

[S7] L. Binci, P. Barone, and F. Mauri, Phys. Rev. B **103**, 134304 (2021).

[S8] O. Bistoni, P. Barone, E. Cappelluti, L. Benfatto, and F. Mauri, 2D Materials **6**, 045015 (2019).

[S9] X. Gonze, B. Amadon, P.-M. Anglade, J.-M. Beuken, F. Bottin, P. Boulanger, F. Bruneval, D. Caliste, R. Caracas, M. Côté, T. Deutsch, L. Genovese, P. Ghosez, M. Giantomassi, S. Goedecker, D. Hamann, P. Hermet, F. Jollet, G. Jomard, S. Leroux, M. Mancini, S. Mazevet, M. Oliveira, G. Onida, Y. Pouillon, T. Rangel, G.-M. Rignanese, D. Sangalli,
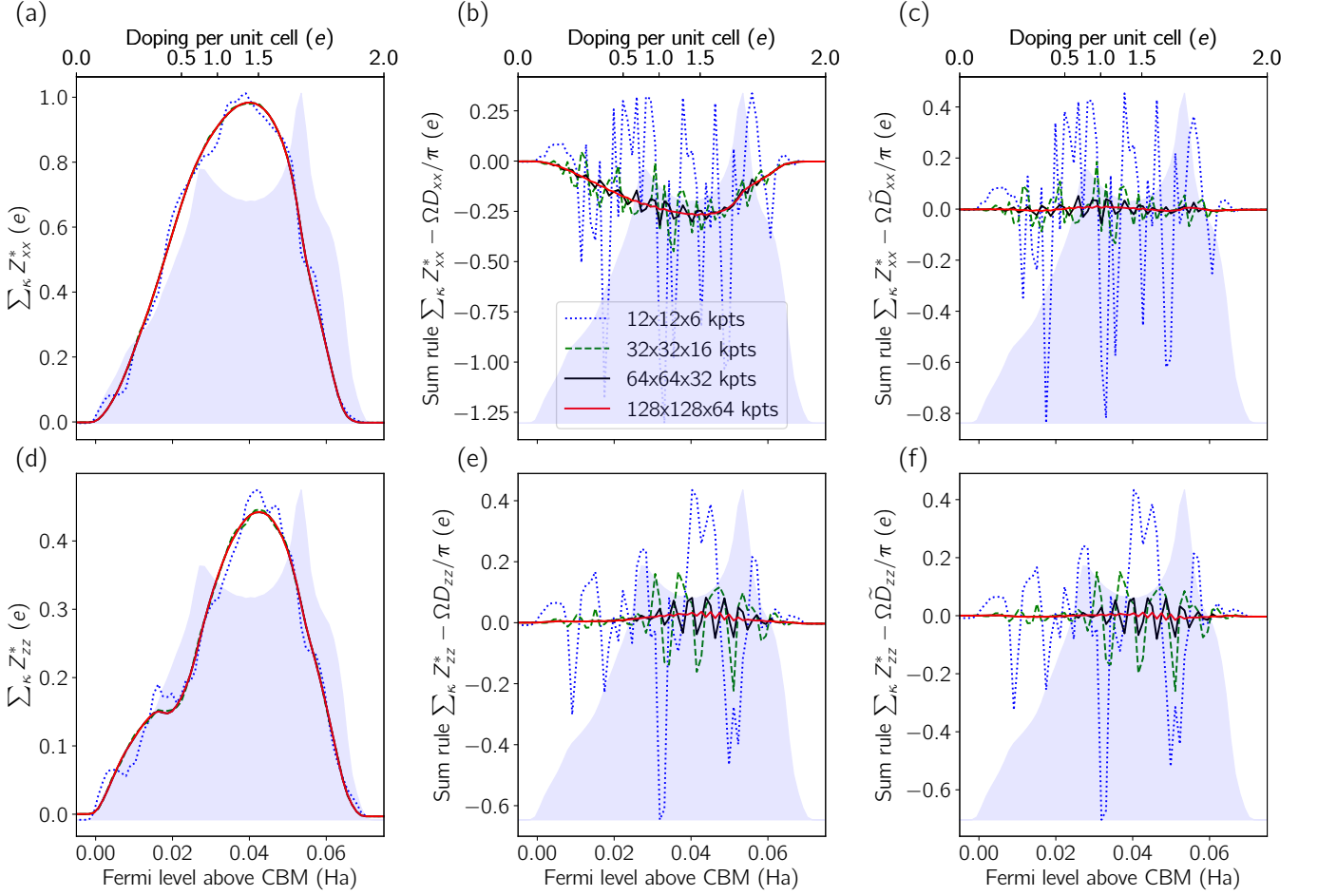
FIG. S11: For SnS$_2$ using different k meshes, sum of nonadiabatic Born effective charges (naBECs) for the (a) xx and (d) zz components; (b) and (e): sum of naBECs and velocity-velocity Drude weight (DW); (c) and (f): sum of naBECs and momentum-velocity version of DW. The Density of states of the isolated conduction band superimposed. $\sigma = 0.001$ Ha for all calculations.

R. Shaltaf, M. Torrent, M. Verstraete, G. Zerah, and J. Zwanziger, Computer Physics Communications **180**, 2582 (2009), 40 {YEARS} {OF} CPC: A celebratory issue focused on quality software for high performance, grid and novel computing architectures.

[S10] D. R. Hamann, Phys. Rev. B **88**, 085117 (2013).

[S11] J. P. Perdew, K. Burke, and M. Ernzerhof, Phys. Rev. Lett. **77**, 3865 (1996).

[S12] J. P. Perdew and Y. Wang, Phys. Rev. B **45**, 13244 (1992).

[S13] A. A. Mostofi, J. R. Yates, G. Pizzi, Y.-S. Lee, I. Souza, D. Vanderbilt, and N. Marzari, Computer Physics Communications **185**, 2309 (2014).

[S14] X. Ge and D. Lu, Phys. Rev. B **92**, 241107 (2015).

[S15] J.-M. Lihm and C.-H. Park, Phys. Rev. X **11**, 041053 (2021).

[S16] C. E. Dreyer, M. Stengel, and D. Vanderbilt, Phys. Rev. B **98**, 075153 (2018).

[S17] C. J. Pickard and F. Mauri, Phys. Rev. Lett. **91**, 196401 (2003).

[S18] S. Ismail-Beigi, E. K. Chang, and S. G. Louie, Phys. Rev. Lett. **87**, 087402 (2001).

[S19] H. Lu, C.-W. Bark, D. Esque de los Ojos, J. Alcala, C. B. Eom, G. Catalan, and A. Gruverman, Science **336**, 59 (2012), http://science.sciencemag.org/content/336/6077/59.full.pdf.